Korean J. Chem. Eng., **21**(2), 352-357 (2004)

Reconstruction Algorithm of Electrical Impedance Tomography for Particle Concentration Distribution in Suspension

Min Chan Kim†, Kyung Youn Kim*, Sin Kim and Kyung Jin Lee****

Department of Chemical Engineering, *Department of Electrical and Electronic Engineering,
**Department of Nuclear and Energy Engineering, Cheju National University, Cheju 690-756, Korea
(*Received 21 February 2003 • accepted 4 August 2003*)

Abstract−An inverse problem is solved to obtain the particle concentration profile in suspension under pressure-driven flow with electrical impedance tomography (EIT). The finite element method (FEM) is employed in the forward problem and the regularized Newton-Raphson iterative method is used in the inverse problem. Different FEM meshes are used in the forward and the inverse problem not to commit inverse crime. To avoid post-calibration of measurement data, the complete electrode model is introduced. For the evaluation of the robustness of the reconstruction algorithm, several testing cases with measurement error are considered. The proposed algorithm can be used to reconstruct the particle concentration in suspension.

Key words: Particle Concentration, Electrical Impedance Tomography, Complete Electrode Model, Inverse Crime, Regularization

INTRODUCTION

The processing of suspension is important in manufacturing of many products such as composite materials, food, paper, and personal care products. Since the particle volume-fraction distribution in suspension has an effect on many rheological properties such as relative viscosity, the information on the particle concentration is essential for understanding the industrial process. Hence, the particle-volume fraction distribution in suspensions has attracted many researchers interest for a long time. Gadala-Maria and Acrivos [1980] observed a decrease of the suspension viscosity in a Couette rheometer due to the change of particle concentration distribution driven by the shear. Later, Leighton and Acrivos [1987] showed experimentally and theoretically that the particles migrate from the higher shear region (inner wall) to the lower one (outer wall) in a Couette rheometer and this migration causes a decrease in the apparent viscosity. Using nuclear magnetic resonance (NMR) imaging, Abotte et al. [1991] found that particles migrate away from the inner cylinder toward the outer wall under the low shear rate in a Couette rheometer. Many other studies on particle migration under shear have been conducted by using NMR images [Chow et al., 1994; Mondy et al., 1994; Corbett et al., 1995] and laser Doppler velocimetry (LDV) [Koh et al., 1994; Lyon and Leal, 1998]. Based on the experimental findings, the first theoretical model for the particle migration under shear was proposed by Leighton and Acrivos [1987]. By extending their model, Phillips et al. [1992] proposed a new constitutive equation, which can describe the actual particle concentration profile. This model predicted the experimental results of particle concentration profile under the Couette and Poiseuille flows quite well.

Recently, EIT technique has been employed to investigate two-phase flow phenomena [Reinecke et al., 1988; Butler and Bonnecase, 1999], because it is relatively inexpensive and has good time resolution even though it has relatively poor spatial resolution with respect to NMR or X-ray CT. Unlike the X-ray CT, the current does not cross the electrodes on the boundary of the system, *i.e.*, the current distribution is a function of impedance distribution inside the system. Because of this fact, the inverse Fourier transform, like that used in other technique, cannot be used in EIT. Then, EIT requires a more sophisticated image reconstruction algorithm than other imaging techniques such as X-ray CT. The data acquisition time and the spatial resolution of EIT system reach a few ms and 5%, respectively [Ovacik and Jones, 1998].

In the present study, a new online-monitoring algorithm to visualize shear-induced particle migration in the pressure-driven flow by the nonintrusive EIT technique is proposed. To overcome the post-calibration of measurement data, a complete electrode model is employed, and to avoid a so-called inverse crime, node-based FEM is used to get the synthetic measurement data, and element-base FEM is used in the reconstruction algorithm. And, to enhance the computational efficiency, different meshes are used in the forward and inverse problems; the Jacobian is calculated by employing the sensitivity method. In order to show the robustness of the proposed reconstruction algorithm, we test several artificial particle concentration distributions.

THEORETICAL BACKGROUND OF EIT SYSTEM

The relationship between the dimensionless conductivity σ_d and volume fraction c_v of nonconducting suspension particles such as plastic bead and gaseous bubble is given as [Meredith and Tobias, 1961]

$$c_v = \frac{24 - (63 + 448\sigma_d + 64\sigma_d^2)^{1/2}}{2(8 + \sigma_d)} \tag{1}$$

where $\sigma_d = \sigma/\sigma_0$ is the ratio of the conductivity of suspension to that of pure liquid. By using the above equation, the conductivities are

†To whom correspondence should be addressed.
E-mail: mckim@cheju.ac.kr

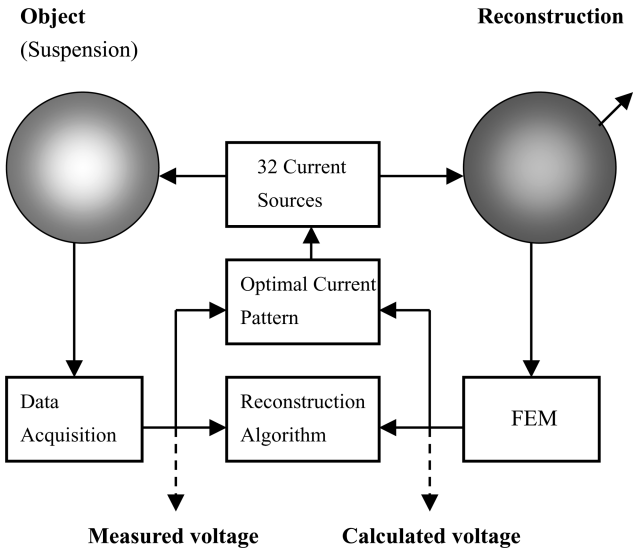

Fig. 1. Schematic diagram of EIT system.

converted into the particle concentrations. In this study, we introduce EIT technique to obtain the particle concentration distribution in suspension.

In the EIT system an array of electrodes is attached on the boundary of an object. Small alternating currents are injected through these electrodes and the resulting voltages are measured. From these boundary measurement data the internal conductivity (or impedance) distribution of the object, that is, the particle concentration distribution, can be obtained. A schematic diagram of the EIT system is shown in Fig. 1.

In terms of mathematics, the EIT reconstruction problem is a nonlinear ill-posed inverse problem. The numerical algorithm, which converts the boundary measurement data to the internal conductivity distribution, consists of iteratively solving the forward problem and updating the conductivity distribution as determined by the formulation of inverse problem. The forward problem of EIT calculates the boundary voltages by using the assumed conductivity distribution, and the inverse problem reconstructs the conductivity distribution by using the boundary voltage measurements. The details of the forward and the inverse problems are discussed below.

1. Forward Problem

When the conductivity distribution σ and boundary current I_l through the l'th electrode are given, the electrical potential distribution u within the problem domain Ω is governed by the following Laplace equation:

$$\nabla\cdot(\sigma\nabla u)=0,\quad x\in\Omega \tag{2}$$

There are several models on the boundary conditions, such as continuum model, gap model, shunt model and complete electrode model [Vauhkonen, 1997]. Among these models, the complete electrode model is the most realistic model that considers the shunt effect of the electrodes and the contact impedances between the electrodes and suspension. In the complete electrode model, the boundary conditions are

$$u+z_l\sigma\frac{\partial u}{\partial \nu}=U_l\quad x\in e_l,\quad l=1,2,\ldots,L \tag{3a}$$

$$\int_{e_l}\sigma\frac{\partial u}{\partial \nu}dS=I_l\quad x\in e_l,\quad l=1,2,\ldots,L \tag{3b}$$

$$\sigma\frac{\partial u}{\partial \nu}=0,\quad x\in\partial\Omega\backslash\cup_{l=1}^{L}e_l, \tag{3c}$$

where e_l is the l'th electrode, z_l is the effective contact impedance between the l'th electrode and the object, U_l is the voltage on electrode e_l, ν is the outward directed normal vector. In addition, the following two conditions for the injected currents and the measured voltages are needed to ensure the uniqueness of the solution:

$$\sum_{l=1}^{L}I_l=0, \tag{4a}$$

$$\sum_{l=1}^{L}U_l=0. \tag{4b}$$

In this study, we inject simple current patterns into 32 electrodes

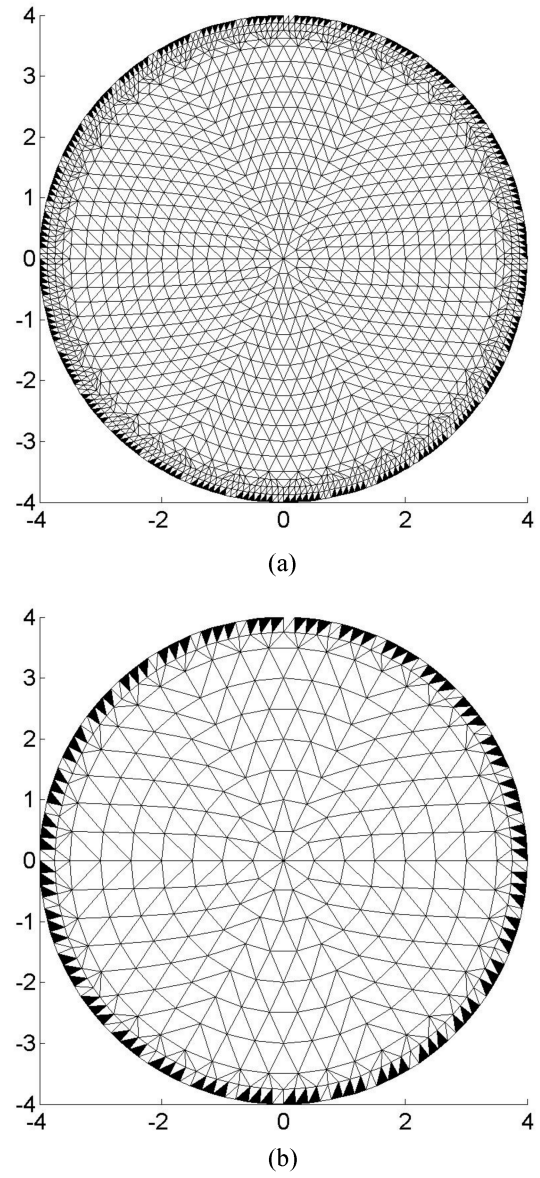

Fig. 2. FEM meshes. (a) mesh used in forward problem, (b) mesh used in inverse problem. Locations and size of the electrodes are marked with darkened elements.

simultaneously as follows:

$$I_l^k = \begin{cases} I_0\cos(k\zeta_l) & l=1, 2, \ldots, 32,\ k=1, 2, \ldots\ 16 \\ I_0\sin(k\zeta_l) & l=1, 2, \ldots, 32,\ k=1, 2, \ldots\ 15 \end{cases} \quad (5)$$

where $\zeta_l=2\pi l/32$. It is known that this current pattern called trigonometric pattern is the best to distinguish a central circular inhomogeneity inside the homogeneous circular conductor. This model has been shown to predict the measured voltages at the precision of the measurement system [Sommersalo et al., 1992]. Therefore, the complete electrode model does not need to be calibrated to the experimental data to account for discrepancies between the experimental measurements and the solution of the forward problem due to the contact impedance and the geometrical mismatches of electrodes position and width between experimental condition and FEM meshes.

Since the above equation cannot be solved analytically for the arbitrary conductivity distribution, a numerical method such as the FEM method should be employed to obtain the solutions. The FEM meshes shown in Fig. 2 are used in this study. As shown in this figure, to obtain boundary voltages accurately, the forward solver will use finer mesh than the inverse solver. Furthermore, if the same mesh and numerical scheme are used both in the simulation of the measurement data and in the solution of the inverse problem, we may commit a so-called inverse crime, where numerical errors may be cancelled out inadvertently. To avoid inverse crime, not only different FEM meshes as shown in Fig. 2 but also different FEM schemes are used. The node-based FEM calculation is used to get the synthetic boundary voltages which are assumed to be the experimental data in the numerical simulation, and element-based FEM is employed in the reconstruction algorithm. In node-based calculation, the continuous conductivity distribution is approximated as:

$$\sigma=\sum_{n=1}^{N}\varphi(x,y)\sigma_n. \quad (6)$$

Here, $\varphi(x, y)$ is the basis function, σ_n is the conductivity at node n and N is the number of nodes. However, in element-based calculation the conductivity distribution is parameterized such that

$$\sigma=\sum_{e=1}^{E}\sigma_e\chi_e, \quad (7)$$

where χ_e is the characteristic function whose values is 1 at the e-th element and 0 at other elements, σ_e is the conductivity at e-th element and E is the number of elements. The details on the numerical solution of the forward problem have been discussed in our previous work [Kim et al., 2003]. Most previous researchers approximated the conductivity distribution as Eq. (7) throughout their works. So, they may have committed an inverse crime.

Butler and Bonnecaze [1999] adopted the EIT for the visualization of the particle shear migration. They assumed the particle concentration within the element was constant and the conductivity values of the elements in any ring were the same. Since they used the shunt and point electrode model, to account the contact impedance and the finite electrode width effect, the measurement data should be calibrated based on the relationship between preliminary experiment data and the synthetic measurements from the forward solution for a homogeneous conductivity. And they might have committed an inverse crime because they used the same FEM mesh and numerical scheme in numerical experiments. In the present study, a complete electrode model which considers the contact impedances between the electrodes and electrolyte and the effect of finite width of electrodes is used, and the conductivity values of elements in any ring are set to the same value to enforce the symmetric conductivity profile. So, the present forward model is more physically realistic than that of Butler and Bonnecaze [1999].

2. Inverse Problem

The inverse problem of EIT maps the boundary voltages from real or artificial experiments to the impedance image. The regularized objective function may be chosen to minimize the squared error,

$$\Phi(\sigma)=[\mathbf{V}-\mathbf{U}(\sigma)]^T[\mathbf{V}-\mathbf{U}(\sigma)]+\alpha[\mathbf{R}(\sigma-\sigma^*)]^T[\mathbf{R}(\sigma-\sigma^*)] \quad (8)$$

where $\mathbf{V}$ is the vector of measured voltage, $\mathbf{U}(\sigma)$ is the calculated boundary voltage vector that must be matched to $\mathbf{V}$, $\mathbf{R}$ is the regularization matrix, α is the regularization parameter and σ^* is the assumed conductivity vector. So, the iterative equation to update the conductivity vector based on the above regularized object function becomes

$$\sigma^{k+1}=\sigma^k+(\mathbf{H}+\alpha\mathbf{R}^T\mathbf{R})^{-1}\{\mathbf{J}^T(\mathbf{U}(\sigma)-\mathbf{V})-\alpha\mathbf{R}^T[\mathbf{R}(\sigma^k-\sigma^*)]\}, \quad (9)$$

where $\mathbf{H}=\mathbf{U}''$ is the Hessian matrix and is approximated as the square of the Jacobian for the computational efficiency. The effect of regularization methods on the quality of reconstructed images is discussed in Kim et al. [2001] for the gas-liquid two-phase flow situation. In the present problem, the conductivity is constrained to be a function of radial position and can be smooth. From this prior information on particle concentration distribution, the first-order difference regularization is employed. In this regularization method, the regularization matrix $\mathbf{R}$ is chosen to be $|\mathbf{R}\sigma|\approx|\nabla\sigma|$, and σ^* is set to 0. In this case, the gradient of the conductivity of the e-th element can be approximated as the differences between the conductivity of e-th element and those of the nearest neighbor elements that share the face of the finite element. A large regularization parameter forces the conductivity distribution to be constant.

In the present case, the particle concentration shows axial symmetric characteristics, so the conductivity values of element in any ring of Fig. 2(a) are set to the same value, and the elements in any ring were grouped into one pseudo-element. The Jacobian and regularization matrices for these pseudo-elements are transformed as

$$\mathbf{J}_G=\mathbf{G}\mathbf{J} \quad (10)$$

$$\mathbf{R}_G=\mathbf{G}^T\mathbf{R}\mathbf{G} \quad (11)$$

where $\mathbf{G}=(G_1, G_2, \ldots G_G)\in\Re^{N\times NG}$, $G_i=(0, 0, \ldots, 0, 1, 1, \ldots, 1, 0, 0, \ldots, 0)^T\in\Re^{N\times 1}$ where 1's are located at the columns where the elements are grouped into the i-th annular, and NG is the number of pseudo-elements. So, the iterative equation to update the conductivity vector for the pseudo-element becomes

$$\sigma_G^{k+1}=\sigma_G^k+(\mathbf{J}_G^T\mathbf{J}_G+\alpha\mathbf{R}_G^T\mathbf{R})^{-1}\{\mathbf{J}_G^T(\mathbf{U}(\sigma)-\mathbf{V})-\alpha\mathbf{R}_G^T\mathbf{R}\sigma_G^k\}, \quad (12)$$

where σ_G is the conductivity vector for the pseudo-element. The initial guess for the conductivity distribution is chosen in the following way. It is assumed that the boundary voltages are decomposed as

$$U_l(\sigma)\approx\frac{\sigma}{\sigma_r}U_l(\sigma_r). \quad (13)$$

where σ_r is an arbitrarily chosen constant conductivity. And, the best homogeneous conductivity σ_0 that minimizes the following functional is obtained by least-square method.

$$\left|\mathbf{V}-\frac{\sigma_0}{\sigma_r}\mathbf{U}(\sigma_r)\right|. \tag{14}$$

In the iteration of the inverse problem, we have to solve the forward problem in order to obtain the boundary voltages and the Jacobian matrix. Much of computation time is consumed in calculating the Jacobian matrix. So, to calculate the Jacobian matrix is one of key factors in the performance of the reconstruction algorithm. The standard finite difference method was employed in most of the previous works. However, by considering the ease of programming and computational speed, we used the sensitivity method based on the Geselowitzs theorem. In our experience, our algorithm based on the sensitivity method is more than 10 times faster than the standard method. And, furthermore by reordering of matrix product, we increased the calculation speed of the Jacobian matrix based on the sensitivity method more than 10 times. So, the speed of the present algorithm to calculate the Jacobian matrix is about 100 times faster than the conventional standard finite difference method, which was used in most of the previous studies [Yorkey et al., 1987; Butler and Bonnecaze, 1999].

In the sensitivity method, the element of the Jacobian matrix is calculated as

$$\frac{\partial U_l^k}{\partial \sigma_n}=\int_{\Omega_n}\nabla u_l\cdot\nabla u_k, \tag{15}$$

where u_l and u_k are the voltage distribution when the l'th and k'th current patterns are used, respectively. The integral of the above equation is calculated in FEM formulation of Eq. (1) as a part of the forward problem.

SIMULATION RESULTS AND DISCUSSION

Unlike many other types of imaging techniques, making general statements about the limitations of imaging with EIT is difficult or impossible. The resolution of the EIT system depends on various variables, such as conductivity contrast and distribution, injected current pattern, and the errors in current injection and voltage measurement. Therefore, to verify the appropriateness of EIT for the present system, a series of simulations should be conducted.

To investigate the effect of the conductivity distribution and the measurement error level on the resolution of reconstructed image, we consider several artificial conductivity distributions and obtain the synthetic boundary voltages by using the forward solver described earlier. And to test the robustness of our algorithm against the measurement error, Gaussian random noise of zero mean is introduced. For the shear-induced particle migration in suspension, the conductivity distribution can be expected to be continuous. The conductivity distribution of the first example shows a monotonic increase from the center to the wall, as shown in Fig. 3. In the second example of Fig. 4, the conductivity distribution shows a minimum point.

As a third example, we consider a particle concentration distribution for a given volume fraction. The particle volume-fraction distribution under the pressure-driven flow has been investigated

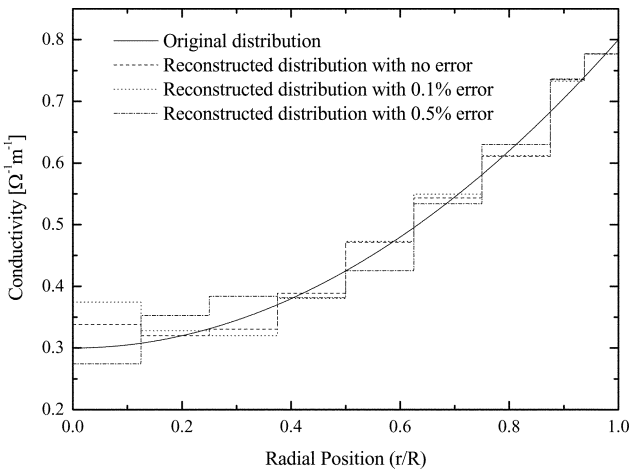

Fig. 3. Computer simulation result for monotonically increasing conductivity profile. The regularization parameter is $\alpha = 10^{-6}$.

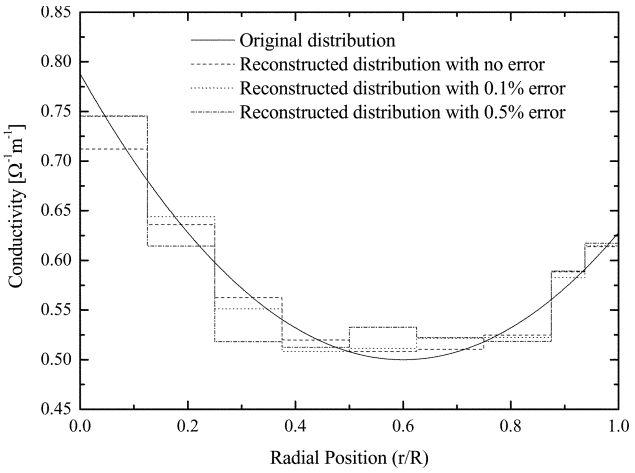

Fig. 4. Computer simulation result for the conductivity profile showing the minimum. The regularization parameter is $\alpha = 10^{-6}$.

theoretically and experimentally. When the volume fraction is given, the particle concentration distribution can be obtained analytically by the diffusion model [Phillips et al., 1992]. Based on the concentration distribution by the diffusion model and Eq. (1), we obtain the original conductivity distribution and then conduct a numerical simulation to reconstruct it. The reconstructed particle concentration distribution for $\langle c_v \rangle = 0.45$ is summarized in Fig. 5.

Hampton et al. [1997] showed in their experiment employing NMR that the particle concentration decreases suddenly near the wall for a certain condition. To simulate this situation, we assumed conductivity profiles as shown in Fig. 6 and reconstructed the conductivity profile. As shown in Fig. 6, the reconstructed profile matches the original profile very well near the wall and the area-averaged conductivity value is reconstructed in the region where the conductivity profile shows a sudden jump. Even though the present reconstruction algorithm is developed for a conductivity profile which is smooth, it can be used for the situation showing a large discontinuity. As shown in Figs. 3-6, the particle concentration distribution

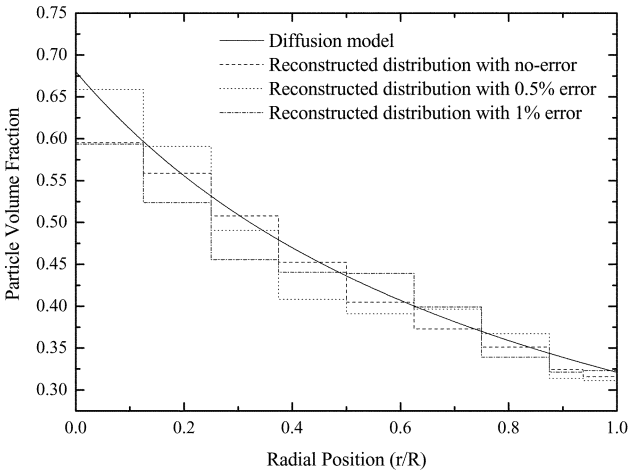

Fig. 5. Reconstructed result based on diffusion model [Phillips et al., 1992] for the case of average volume fraction $\langle c_v \rangle$=0.45. The regularization parameter is $\alpha=10^{-6}$.

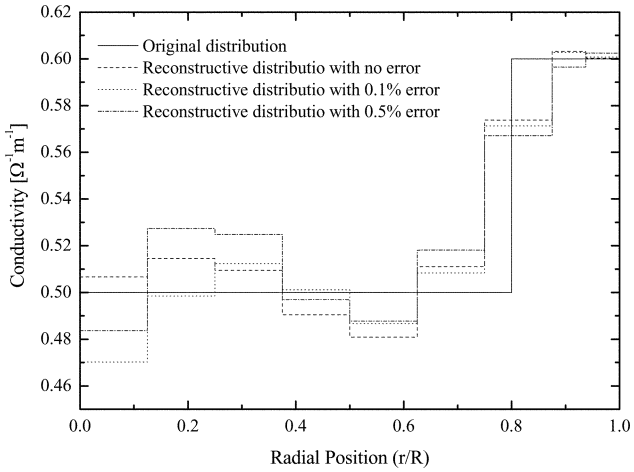

Fig. 6. Computer simulation result for the conductivity profile showing the jump neat the outer wall. The regularization parameter is $\alpha=10^{-6}$.

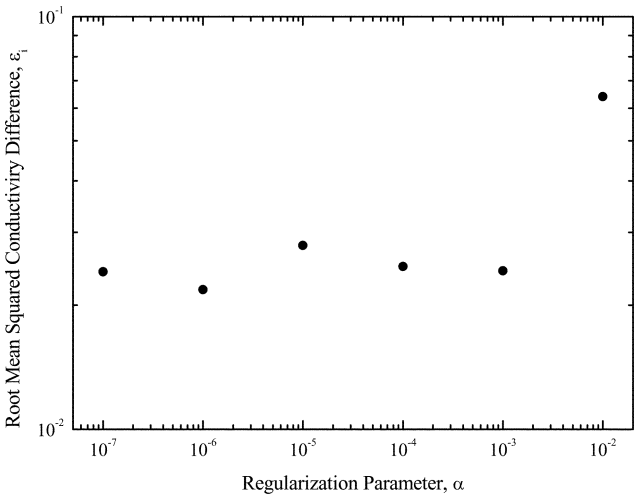

Fig. 7. Root-mean-squared coductivity difference for the second example system (see Fig. 4).

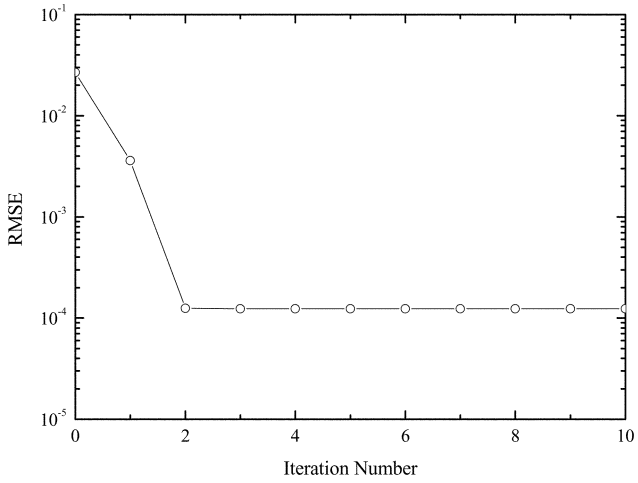

Fig. 8. Root-mean-squared error for the second example (see Fig. 4).

reconstructed by the EIT algorithm is quite reasonable except the inner region, where the discrepancy may be large due to the loose cause (the change of conductivity vector)-and-effect (the boundary voltages) relationship. The small effective area and the distance from the electrodes weaken the cause-and-effect relationship. The reconstructed images show that our algorithm reconstructs the original distribution reasonably and also can treat the measurement errors within the level of 0.5%.

There are several methods for choosing in some sense optimal regularization parameters α. However, the different criteria will yield results of different optimality. Since the true distribution in the simulations was known, the regularization parameters were chosen in such way that the root-mean-squared conductivity difference defined as

$$\varepsilon_i = \sqrt{\frac{(\sigma_o - \sigma)^T (\sigma_o - \sigma)}{\sigma_o^T \sigma_o}} \tag{16}$$

had a minimum value, where σ_o is the original conductivity vector.

For the second example system, ε_i values for the reconstructed conductivities are given in Fig. 7, where ε_i shows minimum at $\alpha=10^{-6}$. So, the regularization parameter is set to $\alpha=10^{-6}$ in all the above examples.

Since in real situations the original conductivity vector is unknown, in other words ε_i cannot be calculated, the root-mean-squared error (RMSE) defined as

$$\varepsilon_v = \sqrt{\frac{(\mathbf{U}-\mathbf{V})^T (\mathbf{U}-\mathbf{V})}{\mathbf{V}^T \mathbf{V}}} \tag{17}$$

is used as the convergence criterion for the inverse problem. If ε_v is less than the predetermined small value, convergence is assumed and the reconstruction algorithm is terminated. For the second example system, RMSE is given in Fig. 8, where RMSE decreases exponentially for the first two iterations, and becomes nearly a constant value after the third iteration. Other examples also exhibit similar trends. Hence, the quality of the reconstructed image does not improve after several iteration steps, and the maximum number of iteration is set to 10.

CONCLUSION

A new EIT algorithm with complete electrode model and trigonometric current pattern is proposed to obtain the particle concentration profile in suspension under pressure-driven flow. Different numerical schemes and FEM meshes were employed to avoid the inverse crime. The robustness of the reconstruction algorithm was verified with several illustrative examples. Considering the computational load and data acquisition time, the convergence rate and the quality of reconstructed images, our algorithm is quite effective compared to the previous ones and can be employed in an on-line measurement system for monitoring the particle concentration in suspension. Therefore, it is expected that the proposed algorithm can be adopted in an on-line monitoring system for the process line where the concentrated suspension plays an important role.

ACKNOWLEDGMENT

This work was supported by Korea Research Foundation Grant (KRF-2002-042-D00029).

NOMENCLATURE

c_v : particle volume fraction
H : Hessian matrix
I : current [A]
J : Jacobian matrix
L : number of electrodes
R : regularization matrix
u : electrical potential [V]
U : calculated boundary voltage vector [V]
V : measured boundary voltage vector [V]

Greek Letters

α : regularization parameter
ε_i : root-mean-squared conductivity difference
ε_v : root-mean-squared global error
σ : conductivity [$\Omega^{-1}m^{-1}$]
σ_d : dimensionless conductivity [-]
Φ : objective function [V^2]

REFERENCES

Abott, J. R., Tetlow, N., Graham, A. L., Altobelli, S. A., Fukushima, E., Mondy, L. A. and Stephens, T. S., "Experimental Observations of Particle Migration in Concentrated Suspensions: Couette Flow," *J. Rheol.*, **35**, 773 (1991).

Butler, J. E. and Bonnecaze, R. T., "Imaging of Particle Shear Migration with Electric Impedance Tomography," *Phys. Fluid*, **11**, 1982 (1999).

Chow, A. W., Sinton, S. W., Iwamiya, J. H. and Stephen, T. S., "Shear-Induced Migration in Couette and Parallel-Plate Viscometers: NMR Imaging and Stress Measurements," *Phys. Fluids*, **6**, 2561 (1994).

Corbett, A. M., Phillips, R. J., Kauten, R. J. and McCarthy, K. L., "Magnetic Resonance Imaging of Concentration and Velocity Profiles of Pure Fluid and Solid Suspensions in Rotating Geometries," *J. Rheol.*, **39**, 907 (1995).

Gadala-Maria, F. and Acrivos, A., "Shear-Induced Structure in a Concentrated Suspension of Solid Sphere," *J. Rheol.*, **24**, 799 (1980).

Hampton, R. E., Mammoli, A. A., Graham, A. L., Tetflow, N. and Altobelli, S. A., "Migration of particles Undergoing Pressure-Driven Flow in Circular Conduit," *J. Rheol.*, **41**, 621 (1997).

Kim, M. C., Kim, S. and Kim, K. Y., "Two Phase Visualization by Electrical Impedance Tomography with Prior Information," *Korean J. Chem. Eng.*, **20**, 601 (2003).

Kim, M. C., Kim, S., Kim, K. Y. and Lee, Y. J., "Regularization Methods in Electrical Impedance Tomography Technique for the Two-Phase Flow Visualization," *Int. Comm. Heat Mass Transfer*, **28**, 773 (2001).

Koh, C. J., Hookham, P. and Leal, L. G., "An Experimental Investigation of Concentrated Suspension Flows in a Rectangular Channel Flow," *J. Fluid Mech.*, **363**, 1 (1994).

Leighton, D. and Acrivos, A., "The Shear-Induced Migration of Particles in Concentrated Suspensions," *J. Fluid Mech.*, **181**, 415 (1987).

Lyon, M. K. and Leal, L. G., "An Experimental Study of the Motion of Concentrated Suspensions in Two-Dimensional Channel Flow. Part 1. Mono-Dispersed System," *J. Fluid Mech.*, **363**, 25 (1998).

Meredith, R. E. and Tobias, C. W., "Conductivities in Emulsion," *J. Electrochem. Soc.*, **108**, 286 (1961).

Mondy, L. A., Brenner, H., Altobelli, S. A., Abotte, J. R. and Graham, A. L., "Shear-Induced Particle Migration in Suspension of Rod," *J. Rheol.*, **38**, 444 (1994).

Ovacik, L. and Jones, O. C., "Development of an Electrical Impedance Computed Tomographic Two-phase Flows Analyzer," USDOE Report, DE-FG07-90ER13032 (1998).

Phillips, R. J., Armstrong, R. C., Brown, R. A., Graham, A. L. and Abotte, J. R., "A Constitutive Equation for Concentrated Suspensions that Accounts for Shear-Induced Particle Migration," *Phys. Fluid.*, **A 4**, 30 (1992).

Reinecke, N., Petritsch, G., Boddem, M. and Mewes, D., "Tomographic Imaging of the Phase Distribution in Two-Phase Slug Flow," *Int. J. Multiphase Flow*, **24**, 617 (1998).

Somersalo, E., Cheney, M. and Isaacson, D., "Existence and Uniqueness for Electrode Model for Electric Current Computed Tomography," *SIAM J. Appl. Math.*, **52**, 1023 (1992).

Vauhkonen, M., "Electric Impedance Tomography and Prior Information," Ph.D. Thesis, Kupio University, Finland (1997).

Webster, J. G., "Electrical Impedance Tomography," Adams Hilger, Bristol (1990).

Yorkey, T. J., Webster, J. G. and Tompkins, W. J., "Comparing Reconstruction Algorithms for Electrical Resistance Tomography," *IEEE Trans. Biomed. Eng.*, **34**, 843 (1987).